PCCP

Accepted Manuscript

ROYAL SOCIETY OF CHEMISTRY

www.rsc.org/pccp

PCCP

PAPER

Effect of nanosize on surface properties of NiO nanoparticles for adsorption of Quinolin-65

Received 00th January 20xx,
Accepted 00th January 20xx

DOI: 10.1039/x0xx00000x

www.rsc.org/

Nedal N. Marei,[ab] Nashaat N. Nassar*[a] and Gerardo Vitale[a]

Using Quinolin-65 (Q-65) as a model-adsorbing compound for polar heavy hydrocarbons, the nanosize effect of NiO nanoparticles on adsorption of Q-65 was investigated. Different-sized NiO nanoparticles with sizes between 5 and 80 nm were prepared by controlled thermal dehydroxylation of $Ni(OH)_2$. The properties of the nanoparticles were characterized by XRD, BET, FTIR, HRTEM and TGA. The effects of the nanosize on the textural properties, shape and morphology were studied. The adsorption of Q-65 molecules onto different-sized nanoparticles was tested in toluene-based solutions. On a normalized surface area basis, the number of Q-65 molecules adsorbed per nm^2 of NiO surface was the highest for NiO nanoparticles of size 80 nm; while 5 nm size NiO nanoparticles was the lowest. Excitingly, the adsorption capacity of other NiO sizes varied from loading suggesting different adsorption behavior, which exhibits the significance of textural properties during adsorption of Q-65. Computational modeling of the interaction between the Q-65 molecule and NiO nanoparticle surface was carried out to get more understanding of its adsorption behavior. A number of factors contributing to the enhanced adsorption capacity of nanoscale NiO were determined. These include surface reactivity, topology, morphology and textural properties.

1. Introduction

Metal-based nanoparticles are emerging as a promising alternative for enhancing heavy oil upgrading and recovery and inhibition of formation damage,[1] through the development of more efficient yet environmentally friendly processes with economical approaches.[2, 3, 4] Because of the 'non-bulk' physical and chemical properties of nanoparticles, nanoparticle surface morphology, structure and reactivity may play roles in different oil and gas processes, such as adsorption and catalysis.[5, 6, 7, 8] Actually, the interactions of nanoparticles with polar heavy hydrocarbon molecules have shown to play an important role in their subsequent processing such as adsorption,[2, 3] post-adsorption thermo-oxidative decomposition,[4, 9] catalytic steam gasification,[10, 11] and enhanced oil upgrading and recovery.[9] Although there is a great deal of interest in the use of nanoparticles as adsorbents and catalysts for enhancing crude oil upgrading and recovery, stabilization of asphaltenes and inhibition of formation damage, the effect of nanoparticle size on their adsorptive and catalytic behavior towards polar heavy hydrocarbons is still unclear. Nanoparticle, defined as a particle that has a characteristic dimension between 1 and 100 nm and has unique properties that are different than the bulk particles with the same chemical composition.[6] We believe here that, despite this broadly accepted definition, within the specified size range of 1 to 100 nm, nanoparticle may undergo dramatic changes in surface properties, topology, morphology and textural properties which consequently impact its surface and interfacial reactivity. The central question here is this: do nanoparticles of size close to 100 nm behave similarly to the particle of size close to 1 nm, with the same chemical composition?

In this study we focus here on metal-based nanoparticles for which there is substantial interest in their application in oil and gas industry.[12, 13, 14, 15, 16] The objective of our study is to investigate the surface characteristics of NiO nanoparticles, which are typically used as adsorbents and catalysts in enhanced heavy oil upgrading and recovery processes.[2, 17, 18, 19, 20] The work aims to investigate the changes in NiO nanosizes and their effects on the properties of the particles itself, including; shape, topology, porosity and surface area. The NiO nanosize effect is demonstrated on the adsorption of model-adsorbing compound for polar heavy hydrocarbons (Quinolin-65), which has shown to be a good model for representing adsorption of asphaltenes.[21, 22] This study provides new understandings on the nanosizes, at the range of 5 to 80 nm, and their effect on the adsorption of heavy hydrocarbons, it also may have important effects on the preparation of advanced nanostructured catalysts and other chemical materials.

2. Experimental work

2.1 Material

A model asphaltene molecule, Quinolin-65 (Q-65) ($C_{30}H_{29}NO_2S$, MW = 467.62 $g.mol^{-1}$, λmax = 375 nm, dye content 80%) purchased from Sigma-Aldrich, Ontario, was used as an

[a] Department of Chemical and Petroleum Engineering, University of Calgary, 2500 University Drive N.W., Calgary, AB. T2N 1N4, Canada
*(Email: nassar@ucalgary.ca, Tel: +1-403-210-9772, Fax: +1-403-210-3973)
[b] Department of Chemical Engineering, An-Najah National University, Nablus, Palestine

adsorbate and model asphaltene molecule. Figure1 shows the chemical structure of Q-65, as drawn with ChemDraw V14.23 From Figure 1, it is observed that this model molecule contain molecular characteristics present in asphaltene fractions reported for Athabasca crude oil, like alkyl chains, aromatic moieties and heteroatoms like sulfur, nitrogen and oxygen. This model molecule represents an asphaltene of the continental type due to the presence of one significant large aromatic area plus side chains per molecule. These facts were confirmed by different authors.[21, 24, 25, 26] Toluene HPLC grade obtained from Sigma-Aldrich, Ontario was used as a solvent. $Ni(NO_3)_2.6H_2O$ obtained from Sigma-Aldrich, Ontario and NaOH pellets obtained from VWR, Radnor, were used as precursors for NiO nanoparticles preparation. All chemicals were used as received without further purification.

2.2 NiO nanoparticles

Controlled thermal dehydroxylation of $Ni(OH)_2$ was used to prepare different sizes of NiO nanoparticles in the range of 5 to 80 nm. The first step was the preparation of the $Ni(OH)_2$ precursor under hydrothermal synthesis conditions. 19.47 g of nickel nitrate ($Ni(NO_3)_2.6H_2O$) was dissolved in deionized water and, after complete dissolution of the nickel salt, NaOH pellets were added pellet by pellet under magnetic stirring until a pH of 11 was reached to precipitate small nickel hydroxide particles ($Ni(OH)_2$). The final slurry mixture was homogenized for 15 min, and then transferred to a polypropylene bottle that was sealed properly to avoid loss of water by evaporation. Then, the slurry was crystallized for 4 h at 373 K in an oven. After crystallization, the product was filtered, washed with distilled water and dried for 12 h at 373 K. The dried material was then calcinied with a ramp of 5 K/min for 2-3 h at different temperatures in the range of 573 to 973 K to get NiO nanoparticles by controlled dehydroxylation of $Ni(OH)_2$ with average crystalline domain sizes from 5 to 80 nm. The nanoparticle crystalline domain sizes increased with increasing the calcination temperature and time.

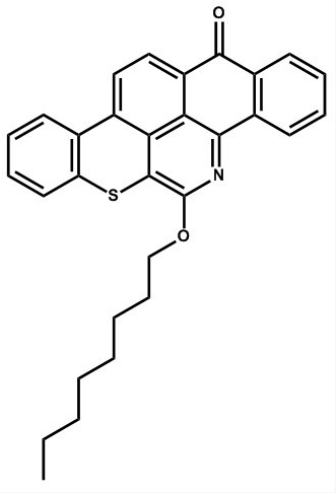

Figure 1. Q-65 molecular structure drawn with ChemDraw V14.[23] The resemblance with a asphaltene molecule can be seen by the archipelago aromatic region, the alkyl chain and the presence of heteroatoms like sulfur, nitrogen and oxygen.

2.3 Characterization of the prepared NiO nanoparticles

2.3.1 X-ray diffraction

Dried powders of nanoparticles were characterized by X-ray diffraction using a Rigaku ULTIMA III X-ray diffractometer with Cu Kα radiation as the X-ray source. The scan was performed in the range 30–90º 2θ using a 0.02º step and a counting time of 1º/min. The crystalline domain sizes were measured using the Debye-Scherrer equation as implemented in the commercial software JADE[27] (provided with the diffractometer), by calculating the full width at half-maximum (FWHM) of the peaks fitting the experimental profile to a pseudo-Voigt profile function.

2.3.2 Textural properties

The surface areas of the prepared nanoparticles were estimated following the Brunauer-Emmett-Teller (BET) method. This was achieved by performing nitrogen physisorption at 77 K, using a Micromeretics Tristar 3000 surface area analyzer, Norcross, GA. The samples were degassed at 423 K under N_2 flow overnight before analysis. An estimation of the particle size (assuming spherical particles) was achieved by using the measured BET area as per eq 1[22]

$$d = \frac{6000}{\mathrm{SA} \times \rho_{NiO}} \quad (1)$$

where *d* is the particle size in nm, SA is the experimentally measured specific surface area (m^2/g), and ρ_{NiO} is the NiO density (6.67 g/cm^3).

2.3.3 High resolution transmission electron microscopy (HRTEM)

High resolution transmission electron microscopy (HRTEM) was performed for the analysis of nanoparticle size, morphology and crystallinity. Around 0.5 mg of NiO nanoparticle sample was dispersed in 1 ml pure ethanol and sonicated for approximately 5 min. For analysis, a drop of this dispersion solution was deposited onto a Formvar/carbon copper grid sample holder. The drop was then allowed to dry depositing NiO nanoparticles on the grid holder. Observations were carried out using a FEI Tecnai F20 FEG TEM with an accelerating voltage of 200 kV.

2.3.4 Infrared analysis

Infrared spectroscopy was performed to study the framework infrared region of the NiO nanoparticles and identify the molecular bonds and functional groups. Approximately 5 mg of nanoparticles was mixed with 500 mg of KBr and the entire mixture was mounted in the DRIFTS sample holder. Analysis was carried out using a Nicolet 6700 FTIR instrument manufactured by Thermo Electron Corporation with a smart diffuse reflectance attachment to carry out DRIFTS (diffuse reflectance infrared Fourier transform spectroscopy). The obtained spectra were the average of 128 scans that were taken for each sample in a range from 400 to 4000 cm^{-1} with a resolution of 2 cm^{-1}.

2.3.5 TGA analysis

Thermogravimetric analysis (TGA) was carried out to identify the hydroxyl group density on the surface of NiO nanoparticles. Approximately 4 mg of NiO nanoparticles were heated from 20 to 800 °C in a thermogravimetric analysis/differential scanning calorimetry (TGA/DSC) analyzer (SDT Q600, TA Instruments, Inc., New Castle, DE) at an air flow rate of 100 cm^3/min and heating rate of 10 °C/min. The TGA instrument was calibrated for mass and heat changes using sapphire as a reference for heat calibration and zinc as a reference for temperature calibration. The surface hydroxyl groups density, σ (#OH/nm^2), of the NiO nanoparticles was calculated using the TGA weight loss between 400 to 800 °C as follows[28, 29]

$$\sigma = 2\frac{W_C/MW}{W_{NP}SA}N_A \quad (2)$$

where W_C is the weight loss (g) from 400-800 °C, W_{NP} is the initial weight of the NiO nanoparticle sample (g), SA is the BET surface area of each NiO nanoparticles (nm^2), the coefficient 2 is employed here since each two hydroxyl group start to condensate above 400 °C to produce a water molecule with molecular weight (MW) of 18.01528 (g/mol), and N_A is the Avogadro's constant.

2.4 Adsorption experiments

Batch adsorption experiments were carried out by exposing 100 mg of each specific NiO nanosize (5 to 80 nm) to a set of tightly sealed 25 mL vials containing final volume of 10 mL solution of Q-65 dissolved in toluene with different initial concentrations ranging from 0 to 0.86 mmol/L at 293 K. The stirring speed was kept constant at 200 rpm for all samples. Samples for analysis were collected after 24 h adsorption, by allowing the nanoparticles containing the adsorbed Q-65 to settle and decanting the supernatant. Some experiments were performed by triplicate, and the standard deviations were calculated and presented. The residual Q-65 concentration in the supernatant was measured using UV-vis spectrophotometry (Evolution 260 Bio UV-Vis spectrophotometer, Thermo Scientific, USA) using a wavelength (λ_{max}) of 375 nm. A calibration curve of the UV−vis absorbance at 375 nm against the Q-65 concentration was established using standard model solutions with known concentrations prepared in-house. UV−vis spectra of the Q-65 solutions were selected based on the absorption linearity range (absorbance < 4.0). The adsorbed amount of Q-65 (molecule of Q-65/nm^2 of nanoparticles) was calculated as shown in eq 3

$$Q = \frac{(C_o - C_e)N_A}{SA}V \quad (3)$$

where Co is the initial concentration of Q-65 in solution (mmol/L), Ce is the equilibrium concentration of Q-65 in the supernatant (mmol/L), V is the solution volume (L), and SA is the BET surface area of NiO nanoparticles (nm^2), NA is the Avogadro's constant.

3. Computational modeling of the interaction of Q-65 molecules with NiO nanoparticles

Computational modeling was carried out to get some insights into the adsorption interaction of the Q-65 molecules with the surfaces of different sizes of NiO nanoparticles. NiO has the rock salt structure (similar to MgO, CaO, CoO and many other binary oxides) and it is of interest because of its relevance to gas sensors, electrochromic coatings, catalysis, and more recently to adsorptive removal of heavy polar hydrocarbons.[1, 22, 30] NiO surfaces have been investigated by computer simulation focusing particularly on low index planes including non-polar and polar surfaces.[31, 32, 33, 34, 35, 36, 37]

Starting from the experimental structural data of NiO within BIOVIA Material Studio Database[38] we created two model of nanoparticles based on the HRTEM images: (a) spherical-like and (b) tablet-like NiO nanoparticles, with similar dimension as those obtained experimentally, to carried out our studies of the Q-65 interaction with these nanoparticles. For our computational studies, we used the modules Forcite and Adsorption Locator included within the commercial modelling software BIOVIA Materials Studio V7.0.[39] BIOVIA Forcite is an advanced classical molecular mechanics tool, designed to work with a wide range of forcefields, allowing fast energy calculations and reliable geometry optimizations of molecules and periodic systems. In our study, BIOVIA Discover module was also used to calculate infrared vibration modes for the NiO structure and BIOVIA Forcite was used to geometrically optimize the Q-65 molecule, to optimize the NiO unit cell and to relax the surface atoms of the created NiO nanoparticle prior to their use on the adsorption study. For the later task, we used BIOVIA Adsorption Location module which is based on simulated annealing (a metaheuristic algorithm for locating a good approximation to the global minimum of a given function in a large search space).[40, 41] Allowing in this way identification of the possible adsorption configurations by carrying out Monte Carlo searches of the configurational space of the nanoparticle of NiO-Q-65 system as the temperature is slowly decreased. To identify additional local energy minima, the process is repeated several times.

Atomistic simulations of inorganic-organic interfaces require accurate description of interatomic forces, and thus, in the present study we employed BIOVIA COMPASS forcefield as it can simulate not only organic molecules but also bulk metal oxides and interfaces between metal oxides and organic molecules.[39, 42] The powerful COMPASS (Condensed-phase Optimized Molecular Potentials for Atomistic Simulation Studies) forcefield has been parameterized and validated by using condensed-phase properties in addition to various *ab initio* and empirical data for molecules in isolation enabling it to accurately and simultaneously make predictions of structural, conformational, vibrational, and thermophysical properties that exit for a broad range of organic and inorganic molecules in isolation and in condensed phases including interfaces and mixtures.[42, 43] Currently, the coverage of this forcefield includes the most common organics, inorganic small molecules, polymers, some metal ions, metal oxides, and metals.[39]

3.1 Q-65 molecule

Q-65 molecule was built and optimized with BIOVIA Forcite before adsorbing it onto NiO nanoparticles. The quality of the Geometry Optimization in BIOVIA Forcite was set to Fine and the Forcefield to BIOVIA COMPASS as this forcefield is compatible with metal oxides[40] and is used to study the interaction of Q-65 with NiO. The optimized Q-65 molecule is presented in Figure 2, where an almost flat configuration of the molecule can be noticed.

3.2 NiO nanoparticles

The experimental structural data for NiO reported in the BIOVIA Materials Studio structural database[39] was transferred to BIOVIA Materials Studio Builder module and the unit cell was geometrically optimized within BIOVIA Forcite. The quality of the Geometry Optimization in BIOVIA Forcite was set to Fine and the Forcefield to BIOVIA COMPASS as this forcefield is compatible with organic molecules, and thus, suitable for studying the interaction of molecules with the NiO surfaces.[42] The experimental unit cell value for NiO is 0.41684 nm[39] and the optimized unit cell value obtained with Forcite and the COMPASS forcefield was 0.41680 nm which is very similar to the experimental one indicating the quality and the reliability of the employed forcefield. The optimized unit cell was then used within BIOVIA Builder module to create two nanoparticles from the optimized structural data using BIOVIA nanostructure builder. The first one was a 5 nm spherical nanoparticle, for this case the internal coordinate atoms in this nanoparticle were fixed to their bulk values and the top layers of atoms (~0.5 nm) which will interact with the Q-65 molecule were allowed to relax under the geometric optimization carried out with BIOVIA Forcite with the BIOVIA COMPASS forcefield which has been parametrized for metal oxides and which is suitable to study interfaces between organics and inorganics.[39, 42] Figure 3a shows the surface relaxed of 5 nm NiO nanosphere. Three facet orientations can be observed in the nanosphere model shown in Figure 3a, the indices of these facets are the {100}, the {110} and the {111} which indicates there are three clear different possible surfaces for adsorption of the Q-65 molecule in the spherical nanoparticle.

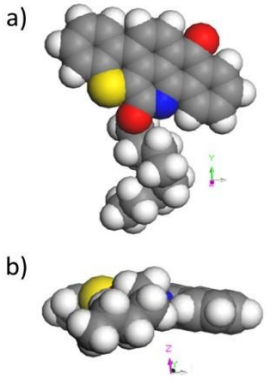

Figure 2. CPK representation of the optimized Q-65 molecule showing its optimized configuration (top and side views, respectively). Grey atoms represent carbon, blue atoms represent nitrogen, white atoms represent hydrogen, yellow atoms represent sulfur and red atoms represent oxygen.

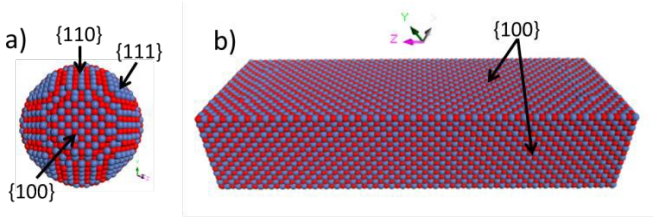

Figure 3. CPK representation, with a 45 degree perspective, of the surface relaxed NiO nanoparticle (the indexes of the exposed facets are indicated). (a) 5 nm NiO nanosphere and (b) 3×5×15 nm NiO nanotablet. Blue atoms represent nickel and red atoms represent oxygen.

The second model was a nanotablet with dimensions 3×5×15 nm and again the top layer of atoms (~0.5 nm) were allowed to relax while the internal atoms were constrained to their bulk values and the geometric optimization was carried out with BIOVIA Forcite with the BIOVIA COMPASS forcefield. Figure 3b shows the surface relaxed NiO nanotablet. For the case of the nanotablet, only the {100} facets are observed, and thus, only one type of surface orientation is available for the adsorption of Q-65 molecules.

3.3 Interaction of Q-65 molecule with NiO nanoparticles

BIOVIA Adsorption locator module was used to gain insights into the interaction of Q-65 molecule with the surfaces of the spherical- and tablet-like nanoparticles built before, which are more representative of the actual used nanoparticles (HRTEM images). The simulating annealing task in BIOVIA Adsorption Locator calculation was set to a quality of Fine (energy cutoff of 1.0×10^{-4} kcal/mol) using the Smart algorithm. The atom based summation method was used for the electrostatic and van der Waals with a cubic spline truncation and a cutoff distance of 1.55 nm. The forcefield selected was BIOVIA COMPASS, which is suitable to study interfaces between organics and inorganics.[39, 42] The top layer atoms (~0.5 nm) in the spherical and the tablet-like nanoparticle surfaces were selected for the interaction with Q-65 molecules, and the maximum adsorption distance value was 1.5 nm with a fixed energy window of 10 kcal/mol for sampling configurations which differ from the lowest configuration in that maximum amount. Several tests were carried out, one with loading a single Q-65 molecule and others with loading several Q-65 molecules on each nanoparticle surface.

4. Results and Discussion

4.1 Characterization studies

4.1.1 X-ray diffraction

X-ray diffraction analysis of the different sizes nanoparticles (Figure 4) confirmed that the correct structure was NiO, as all the XRD patterns match very well with the diffraction peaks of the NiO structure identified in the JADE program, using the database of Materials Data XRD Pattern Processing Identification & Quantification (PDF#01-075-0269). This indicates the preparation of pure NiO nanoparticles. Diffraction peaks around 37.2°, 43.3°, 62.9°, 75.39°, and 79.4° can be indexed as diffraction from (111), (200), (220), (311), and (222)

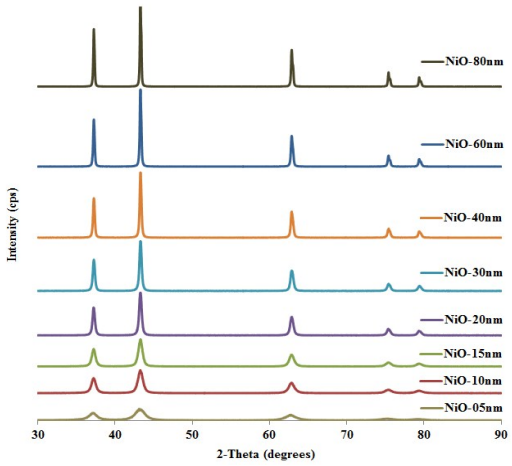

Figure 4. X-ray diffraction powder patterns in the region 30–90º of the prepared NiO nanoparticles at diameter size of 5, 10, 15, 20, 30, 40, 60 and 80 nm.

planes of NiO with cubic structure, respectively. As seen, the peaks are very broad indicating that the prepared nanoparticles have indeed very small crystalline domain sizes (the domain sizes range from 5 to ~80 nm). In addition, the intensity and sharpness of the diffraction peaks were significantly increased as the nanosize of the particle increased. The crystalline domain sizes of the nanoparticles derived from the different diffraction planes using the Debye-Scherrer equation are shown in Table 1.

4.1.2 Textural properties

Table 1 lists the used calcination temperatures and times, X-ray crystalline size and BET surface areas of the prepared NiO nanoparticles. As expected, the surface area of the nanoparticle decreased as the NiO nanosize increased. However, the expected surface area value for each nanoparticle, based on the X-ray crystalline domain sizes, is lower when compared to the ones obtained experimentally, suggesting a possibility of particle aggregation. Figure 5 shows the nitrogen physisorption isotherms for each nominal size of prepared NiO nanoparticles.

Table 1. NiO nanosizes calcination temperature and time, XRD crystalline size, BET surface areas and surface hydroxyl density results.

Calcination temperature (K°)		573	673	723	773	823	873	873	973
Calcination time (h)		2	2	2	2	2	2	3	2
Nominal NiO size (nm)		5	10	15	20	30	40	60	80
X-ray Diffraction planes	111	5	12	15	26	30	43	58	84
	200	5	11	15	25	30	45	63	98
	220	5	10	12	22	26	38	52	73
	311	4	10	12	22	25	36	54	75
	222	4	9	12	21	24	35	48	64
Average crystalline domain size (nm)		5	10	13	23	27	39	55	78
Standard Deviation		0.5	1	2	2	3	4	6	13
Measured BET area (m^2/g)		158	58	42	20	17	11	7	3
Expected particle size by BET (nm) (by equation 1)		6	16	21	45	53	82	129	300
Surface hydroxyl density σ (#OH/nm^2)		8.5	6.3	6.0	6.3	5.9	1.8	1.9	1.1

The International Union for Pure and Applied Chemistry (IUPAC) has classified the adsorption-desorption isotherms in six categories (*Types I to VI*) and the possible hysteresis loops in these isotherms in four categories: *Types H1 to H4*.[44] According to these classifications, *Type IV* isotherm could be the most descriptive in case of all NiO nanosizes as presented in Figure 5. It is known that NiO nanoparticle is a non-porous material, and thus, the presence of a hysteresis loop suggests that the small nanosizes are producing interparticle porosity which is observed by the hysteresis loop formation. Then, the real form of the isotherm should be the reversible *Type II* isotherm that is obtained with non-porous or macroporous adsorbents as in the case of NiO, however, the small sizes of the particles generate interparticle cavities of mesoporous sizes that produce capillary condensation which takes place in these mesoporous generated by the interparticle cavities. The *Type H3* loop is the one that best describe the hysteresis loop observed in the isotherms of the prepared NiO nanoparticles. The desorption of N_2 on NiO nanoparticles which does not exhibit any limiting adsorption at high p/p_o is normally observed with aggregates of plate-like particles which gives rise to slit-shaped pores. This feature begins to disappear with increasing the nanosize as there is no significant hysteresis loops in the case of 40, 60 and 80 nm (Figure 5). The last observation indicates that the largest particles begin to behave more similar to what is expected for a non-porous bulk NiO material, as the original small particles were fused to form the large ones that do not produce interparticle cavities of mesoporous dimensions (between 2 and 50 nm) only interparticle cavities of macroporous dimension (> 50 nm) which do not form hysteresis loops with N_2 physisorption.[45]

4.1.3 Size and morphology of different crystal size of NiO

HRTEM was carried out to get insights into the morphology and sizes of the prepared NiO nanoparticles. Figure 6 shows HRTEM images of different sizes of NiO nanoparticles. As seen, small nanosizes (like 5, 10 and 15 nm) seem to be connected and aggregated forming rod-like morphology. However, the selected area electron diffraction pattern of these samples (Figure 7) indicate that they are indeed composed of very small crystalline domains as these solids produce circular electron diffraction halos. Clear diffraction dots are observed in the selected area electron diffraction images as the crystalline domains get bigger.

In the case of the 20 and 30 nm size nanoparticle (Figure 6) they seem to be formed of flat thin sheets connected to each other, and thus, giving the Type *H3* hysteresis loop observed in the N_2-physisorption isotherms discussed previously. On the other hand, for bigger nanosizes (like 40, 60 and 80 nm), they seem to be formed of more likely sheets with different shapes, while the morphology of the 40 nm sample looks like cylinders, the 60 nm sample are single thicker sheets and the 80 nm sample clearly appear having hexagonal shapes. These observations also help to understand the hysteresis loops and their differences observed in the N_2-physisorption isotherms discussed before.

4.1.4 FTIR analysis

Figure 8 shows the FTIR spectra of NiO nanoparticles having different sizes in the framework region (Figure 8a) and in the hydroxyl stretching region (Figure 8b). The broad absorption

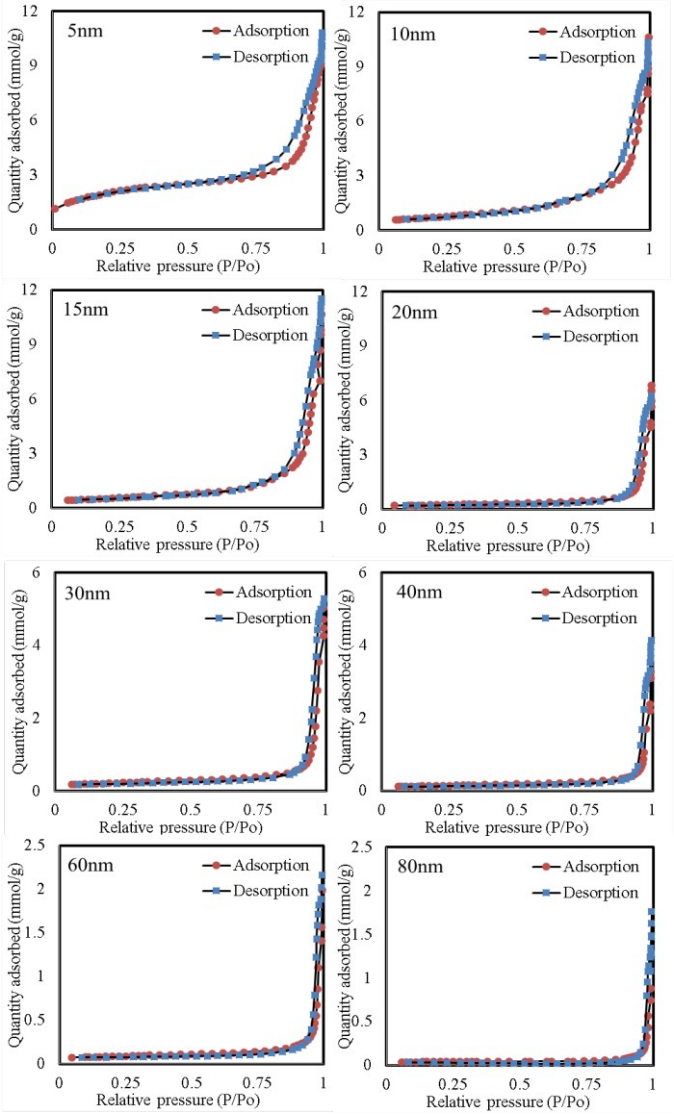

Figure 5. Nitrogen adsorption–desorption isotherms for NiO of different Nanosizes (5-80 nm).

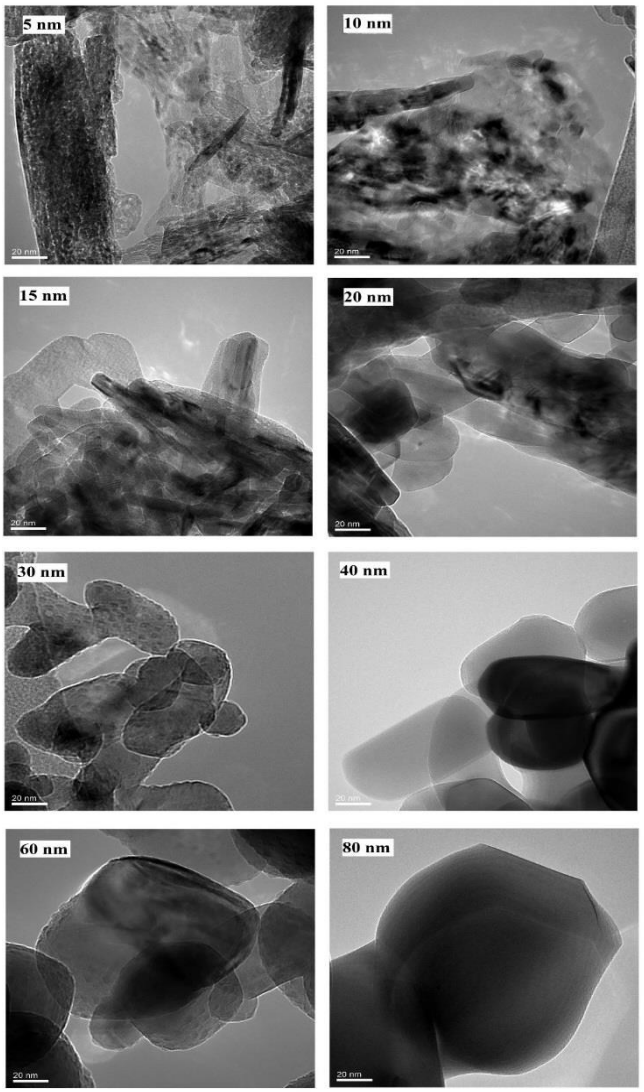

Figure 6. HRTEM images of NiO nanoparticles synthesized with nominal sizes from 5 to 80 nm (the scale mark is 20 nm for all the images).

band in the region of 400–600 cm^{-1} (framework vibration) is assigned to Ni–O stretching vibration mode; the broadness of the absorption band indicates that the NiO powders are nanocrystals.[46] Interestingly, it can be observed in Figure 8a that as the nanoparticles increase in size from 5 to 80 nm the main peak (centered at around 425 cm^{-1} very similar to the value of 422.7 cm^{-1} calculated with BIOVIA Discover module) becomes broader. This has been observed for NiO nanoparticles with sizes between 4 and 16 nm.[46] In the smaller nanoparticles, a shoulder around 550 cm^{-1} is observed, but as the nanoparticles increase in size this band becomes more intense, and in the case of the larger nanoparticles the intensity is similar to the band centered at around 425 cm^{-1}. These two bands together produce a broader band which is centered at around 467 cm^{-1}.

Besides the observed Ni–O vibration in Figure 8a, it is possible to see a broad band centered around 1400 cm^{-1} that should be assigned to –O–H bending vibrations modes. As expected, the smaller the nanoparticle, the more –OH present on its surface and consequently the larger the bending vibration, as observed for the 5 nm size NiO nanoparticles in Figure 8a. In support of this, Figure 8b shows the –OH stretching vibration which is more intense in the smaller NiO nanoparticle (5 nm). This high –OH density for the small 5 nm particles should affect their surface interaction with Q-65 molecule.

4.1.5 Surface hydroxyl density

To estimate the content of hydroxyl group on the surface of each sizes of nanoparticles, thermogravimetric analysis was carried out. Figure 9 shows the thermograms for the different sizes of NiO nanoparticles. The TGA curves were divided into three regimes:[28, 47, 48] a) 25 °C to 100 °C, related to gas desorption; b) 100 °C to 400 °C, where the higher mass loss shown here due to the desorption of physically adsorbed water molecules; and c) 400 °C to 800 °C, linked to the dehydroxylation of adjacent –OH groups on the surface and their condensation as a water molecules**,** as shown in Figure 10. The weight loss of each NiO nanosizes, at regime c, was used to calculate the hydroxyl density using eq 2 and their values are summarized in Table 1. As seen in Figures 8b, 9 and Table 1 the smallest nanoparticles, i.e. 5 nm, portray the highest hydroxyl surface density which was found to be 8.5 OH/nm2, and this

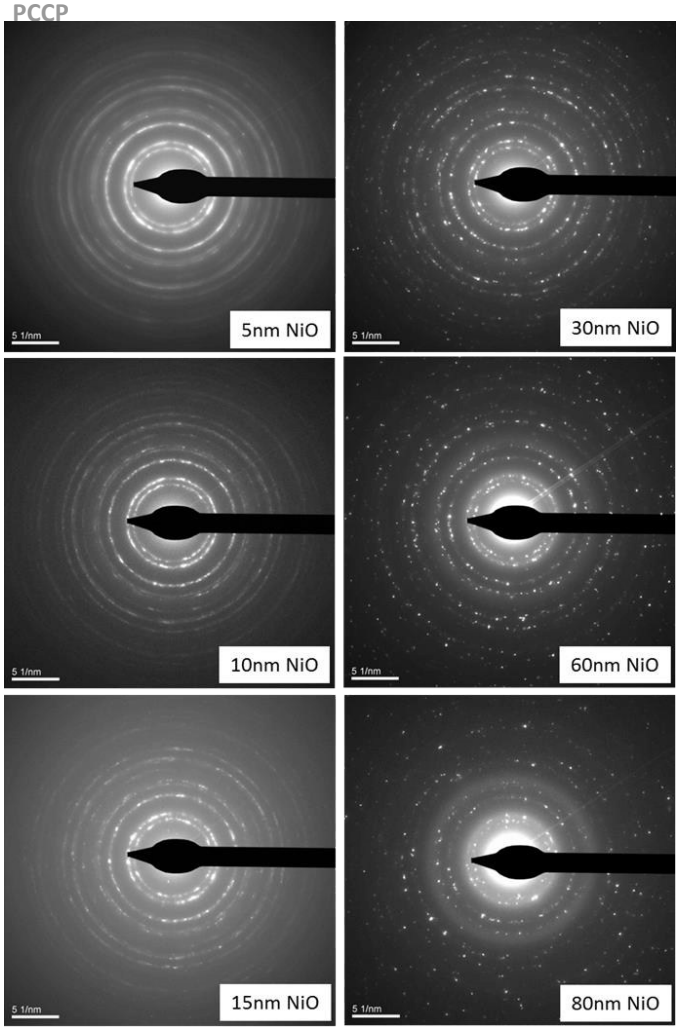

Figure 7. Selected Area Electron Diffraction of NiO nanoparticles synthesized with nominal sizes from 5 to 80 nm (the scale mark is 5 nm^{-1} for each image)

density tends to decrease with increasing the particle size up to 80 nm, having the lowest density value of 1.1 OH/nm2. The quantitative hydroxyl density obtained for the different sizes of NiO agrees very well with the qualitative FTIR analysis discussed before. These observations support the evidence to the effect of high hydroxylation of the surface in the oxide nanostructure as the size gets smaller.

4.2 Computational modeling for adsorption of Q-65 molecules onto NiO nanoparticles

As described before, calculations of the adsorption of Q-65 molecules onto a 5 nm spherical NiO nanoparticle (closest to the actual size obtained experimentally for the real used small nanoparticles) were carried out to get some atomistic insight on the complex interaction of Q-65 molecules with the surfaces of NiO nanoparticles. Figure 11 illustrates the adsorption of one molecule (a), 10 molecules (b) and 80 molecules (c) of Q-65 onto the 5 nm spherical NiO nanoparticle. Figure 11a shows that the lowest configuration of one Q-65 molecule onto the spherical NiO nanoparticle is almost a flat one with the alkyl chain pointing upwards anchored by the interaction of the aromatic rings with the surface having the facet index {110} and having an adsorption energy of -433.2 kcal/mol.

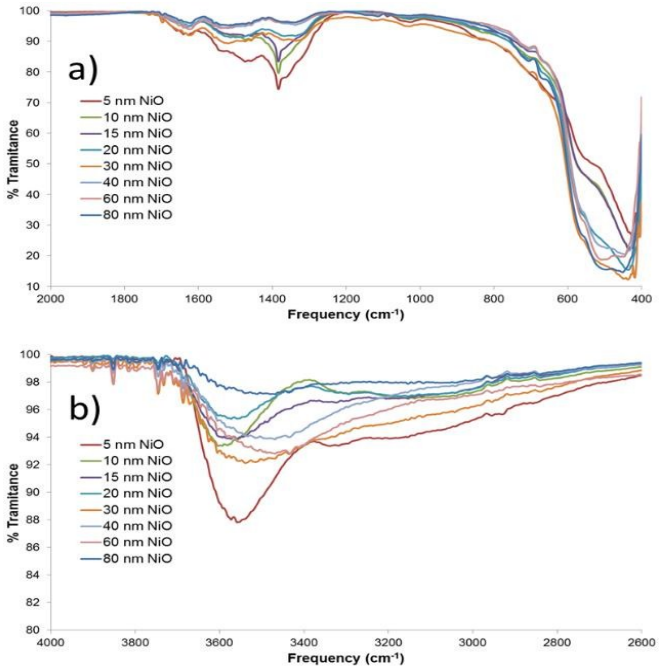

Figure 8. FTIR spectroscopy of the NiO nanoparticles 5-80 nm: a) framework region and b) hydroxyl region.

In Figure 11b, it is observed that as more Q-65 molecules are added (in this case 10), the vertical tilting of some of the Q-65 molecules is observed as compared when only one molecule of Q-65 is alone onto the nanoparticle surface. As more Q-65 molecules are adsorbed (80 molecules in Figure 11c), the lowest configuration order indicates that most of the molecules tend to be adsorbed in a vertical tilted form. This arrangement indicates that more Q-65 molecules can be adsorbed on the surface than it would be estimated by the flat configuration of the molecule, for this case, 1.1 molecules/nm^2 was estimated for the surface saturation in the spherical particle, pointing out the importance of surface morphology for Q-65 adsorption.

Following the findings above, and taking into account that the HRTEM images indicated that some NiO nanoparticles possessed a tablet-like morphology, hence the interaction of Q-65 molecules with a nanotablet of NiO ($3 \times 5 \times 15$ nm dimensions) were carried out and the lowest energy configurations of Q-65 on this nanoparticle are presented in Figure 12. In the used nanotablet of NiO, in the lowest energy configuration found, one Q-65 molecule adsorbs on the only type of surface exposed {100} in an almost flat configuration with the alkyl chains pointing upwards as in the case of the nanosphere by interaction of the aromatic rings with the surface (Figures 12a); however, in this case the adsorption energy is -668.2 kcal/mol which is 235 kcal/mol lower than in the spherical nanoparticle. These results indicate that the morphology of the nanoparticles (exposed facets) will have an effect in the adsorption and catalytic behavior of the nanoparticles being composed of the same chemical elements (nickel and oxygen in this case). When a few more Q-65 molecules are added (10 molecules as observed in Figure 12b), the configuration of the molecules still resembles the almost flat one observed when only one molecule is adsorbed. This is

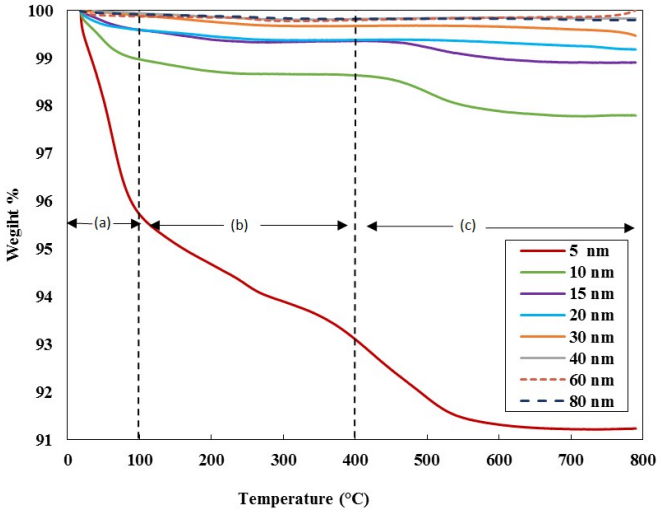

Figure 9. TGA thermograms of different sizes of NiO nanoparticles, with three mass regimes: a) gas desorption b) water molecules desorption c) dehydroxylation adjacent –OH groups.

different to the observation in the case of nanosphere where the vertical tilted configuration seems to be the dominant one, pointing out the importance of surface

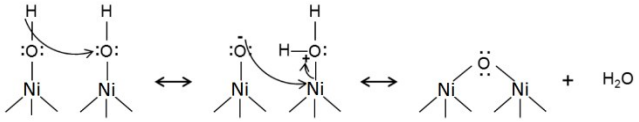

Figure 10. Pictorial representation of the dehydroxylation concept.

4.3 Adsorption isotherms

To validate the findings of computational modeling and to better understand the adsorption of Q-65 molecules on different sizes of NiO nanoparticles, macroscopic solution phase adsorption isotherms were performed to quantify surface coverage on these different-sized nanoparticles. The adsorption isotherms of Q-65 molecules onto different sizes of NiO nanoparticles are shown in Figure 13.

For all cases, the Langmuir and Freundlich adsorption models, represented by eqs 4 and 5, respectively,49, 50 fit to the experimental data

$$Q_e = \frac{Q_{max} K_L C_e}{1+K_L C_e} \quad (4)$$

$$Q_e = K_F C_e^{1/n} \quad (5)$$

where Q_e is the number of Q-65 molecules adsorbed onto the nanoparticles (molecule/nm^2), C_e is the solution phase equilibrium concentration (molecule/L), K_L is the Langmuir adsorption equilibrium constant related to the affinity of binding sites (L/molecule), Q_{max} is the maximum number of Q-65 molecules adsorbed for complete monolayer coverage (molecule/nm^2), and 1/n and K_F are Freundlich constants which are related to the adsorption affinity and adsorbed amount, respectively. Both Langmuir and Freundlich model parameters were estimated by minimization of the sum of squares of the differences between the experimental values and the predicted

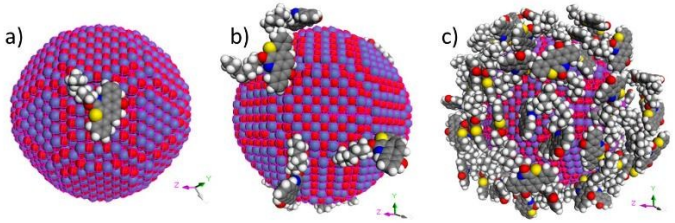

Figure 11. CPK images, with a 45 degree perspective, of the adsorption of Q-65 on the surfaces of a 5 nm NiO spherical nanoparticle. (a) adsorption of one molecule of Q-65 on the 5 nm NiO nanoparticle; (b) adsorption of 10 molecules of Q-65 on the 5 nm NiO nanoparticle; and (c) adsorption of 80 Q-65 molecules on the 5 nm spherical NiO nanoparticle. Bright blue atoms represent nitrogen, yellow atoms represent sulfur, gray atoms represent carbon, white atoms and the red atoms represent oxygen.

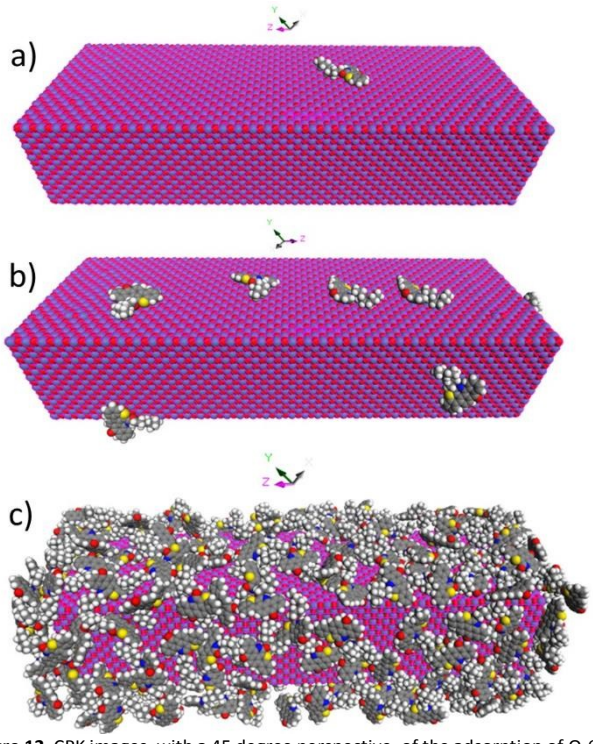

Figure 12. CPK images, with a 45 degree perspective, of the adsorption of Q-65 on the surfaces of a nanotablet (3x5x15 nm) of NiO. (a) adsorption of one molecule of Q-65 on the NiO nanotablet; (b) adsorption of 10 Q-65 molecules on the nanotablet of the NiO nanoparticle; and (c) adsorption of 250 Q-65 molecules on the nanotablet of NiO nanoparticle. Bright blue atoms represent nitrogen, yellow atoms represent sulfur, gray atoms represent carbon, white atoms represent hydrogen, red atoms represent oxygen, light blue atoms represent nickel and pink wireframe indicates the targeted atoms for the adsorption interaction on the surface.

ones using the Solver features in Excel 2015. The non-linear Chi-square analyses,

$$\chi^2 = \sum \frac{(Q_e - Q_{eModel})^2}{Q_{eModel}}$$

was used to evaluate the goodness of fitting results; where Q_e and Q_{eModel} are the adsorbed number of Q-65 molecules obtained experimentally and from modeling, respectively.

Table 2. Estimated Langmuir; K_L (L/molecule), Q_{max} (molecule/nm^2) and Freundlich parameters; 1/n (unit less), K_F [(molecule/nm^2)(L/molecule)$^{1/n}$] for Q-65 adsorption in solution at different NiO nanosizes.

Nominal NiO size (nm)	Langmuir			Freundlich		
	KL ×1015 (L/molecule)	Qmax (molecule /nm^2)	χ^2	KF×10^{10} [(molecule/nm^2) (L/molecule)1/n]	1/n (unitless)	χ^2
5	1.2810	0.2055	0.0020	0.0134	0.7303	0.0190
10	1.4630	0.6869	0.0010	1.3023	0.6317	0.0033
15	1.6072	1.0065	0.0013	0.3247	0.6797	0.0025
20	1.9168	0.7559	0.0068	0.9509	0.6317	0.0086
30	1.8223	0.4654	0.0017	1.7546	0.5156	0.0021
40	0.7552	0.8084	0.0016	1.2361	0.6273	0.0066
60	0.9384	0.9577	0.0037	0.9913	0.6431	0.0044
80	0.5141	1.9156	0.0042	0.0465	0.7417	0.0048

The good fitting to the experimental data was indicated by the low Chi values. Table 2 lists the estimated values of the model parameters.

Clearly, for all NiO nanosizes, the Langmuir model presented a better fitting to the experimental data. This suggests that the selected nanoparticles portray saturation surface coverage. Furthermore, the data showed that, when normalized to BET surface area, there are significant differences in the adsorption of Q-65 molecules from toluene onto different-sized nanoparticles. Both Langmuir parameters (i.e., K_L and Q_{max}) differ with changing of particle size, indicating some differences in the adsorption of Q-65 molecules on the different-sized nanoparticles. Looking at Figure 13, it is evidently noted that the largest particle size has the highest uptake of Q-65 molecules under the tested conditions (1 molecule/nm^2 at the highest concentration tested). On the other hand, the smallest particle size has the lowest uptake, around 0.15 molecules/nm^2.

For the other sizes, the uptake at the highest concentration of Q-65 in the solution seems to be between 0.35 and 0.7 molecules/nm^2, which are lower than the estimated values of 0.9-1.1 molecules/nm^2 obtained by the computational modeling. These experimental results confirm the importance of the nanoparticle surface topology and morphology on its adsorption of organic molecules. Variations on adsorption behavior of different-sized NiO nanoparticles towards Q-65 must then be expected, as different shapes and topologies are found in the particles forcing the adsorption of less Q-65 molecules than theoretically expected. Infrared spectra (Figure 8b) and the TGA estimated density of hydroxyl groups showed that the smaller the nanoparticle the higher the hydroxyl density, thus, this chemical modification of the surface topology may also be contributing to the lower adsorption of Q-65 molecule on the surface of the smallest nanoparticles by changing the interaction of the particle with the organic molecule, and forcing less Q-65 molecules to be adsorbed. Larger flat surfaces seems to have the required adsorption sites to organize quite well big bulky molecules on their top. Hence, larger nanoparticles with extended flat surfaces can adsorb better more molecules. However, if the molecules are very small the trend may change, and thus, it is very important to understand not only the prepared nanoparticle size, topology and morphology, but also the selected molecule for their interaction.

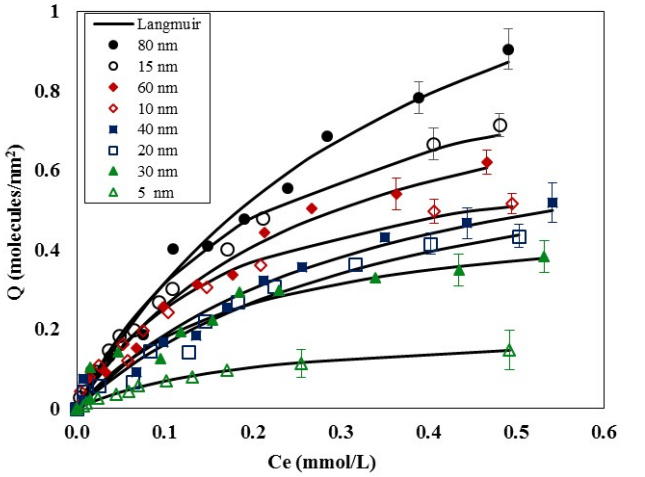

Figure 13. Effect of NiO nanosize on Q-65 adsorptive removal. Experimental conditions are nanoadsorbent dose, 10 g/L; shaking rate, 200 rpm, contact time = 24 h. The symbols are experimental data, and the solid lines are from the Langmuir model (eq 4).

Conclusion

This study is a first attempt to investigate the nanosize effect of nanoparticles toward adsorptive removal of asphaltene model molecule (like Quinolin-65, Q-65) from oil matrix. Different-sized NiO nanoparticles ranges from 5 to 80 nm were prepared in-house using the controlled thermal dehydroxylation method. The HRTEM images showed different shapes of the nanoparticles with different sizes. FTIR analysis identified the difference of the framework group and the hydroxyl density with different nanosizes. TGA analysis showed that the higher the nanosize the less the hydroxyl surface content, which provides more chances for the Q-65 molecules to be adsorbed and attached on the surface. The results of experimental adsorption isotherms support the characteristic studies and confirmed that NiO nanoparticles with 80 nm size have the highest adsorption capacity (molecule/nm^2), while 5 nm size particles have the lowest. Computational modeling was employed to get better insight on the Q-65 interaction with NiO nanoparticles with the assumption of spherical or tablet-like shape nanoparticles. The results clearly indicate that, upon changing the nanosize between 5 and 80 nm, NiO nanoparticles undergo dramatic changes in surface properties, topology, morphology and textural properties which consequently impact their interfacial reactivity and adsorption behavior. We foresee that this size-dependent changes in morphology and textural properties will strongly affect the nanoparticle interfacial reactivity and its application in the oil and gas industry, particularly concerning their surface reactivity in enhancing crude oil upgrading and recovery and inhibition of formation damage.

Acknowledgement

The authors are grateful to the Natural Sciences and Engineering Research Council of Canada (NSERC), Nexen-CNOOC Ltd, and Alberta Innovates-Energy and Environment

Solutions (AIEES) for the financial support provided through the NSERC/NEXEN/AIEES Industrial Research Chair in Catalysis for Bitumen Upgrading. Also, the contribution of facilities from the Canada Foundation for Innovation, the Institute for Sustainable Energy, Environment and Economy, the Schulich School of Engineering and the Faculty of Science at the University of Calgary are greatly appreciated. A special acknowledgement to Dr. Tobias Fürstenhaupt for access to the Microscopy and Imaging Facility of the Health Science Center at the University of Calgary, which receives support from the Canadian Foundation for Innovation and the Alberta Science and Research Authority.

References

1 R. Hashemi, N. N. Nassar and P. P. Almao, Applied Energy, 2014, 133, 374-387.
2 N. N. Nassar, A. Hassan and P. Pereira-Almao, Energy & Fuels, 2011, 25, 1017-1023.
3 J. J. Adams, Energy & Fuels, 2014, 28, 2831-2856.
4 N. N. Nassar, A. Hassan, L. Carbognani, F. Lopez-Linares and P. Pereira-Almao, Fuel, 2012, 95, 257-262.
5 A. El-Qanni, N. N. Nassar, G. Vitale and A. Hassan, J Colloid Interface Sci, 2016, 461, 396-408.
6 M. Auffan, J. Rose, J. Y. Bottero, G. V. Lowry, J. P. Jolivet and M. R. Wiesner, Nature nanotechnology, 2009, 4, 634-641.
7 H. D. Jang, S. K. Kim and S. J. Kim, Journal of Nanoparticle Research, 2001, 3, 141-147.
8 S. Yean, L. Cong, C. T. Yavuz, J. T. Mayo, W. W. Yu, A. T. Kan, V. L. Colvin and M. B. Tomson, Journal of Materials Research, 2005, 20, 3255-3264.
9 R. Hashemi, N. N. Nassar and P. P. Almao, Energy & Fuels, 2013, 27, 2194-2201.
10 A. Hassan, L. Carbognani-Arambarri, N. N. Nassar, G. Vitale, F. Lopez-Linares and P. Pereira-Almao, Appl Catal a-Gen, 2015, 507, 149-161.
11 N. N. Nassar, A. Hassan and P. Pereira-Almao, Energy & Fuels, 2011, 25, 1566-1570.
12 D. D. Zhang, D. L. Wei, Q. Li, X. Ge, X. F. Guo, Z. K. Xie and W. P. Ding, Scientific Reports, 2014, 4, 4021.
13 M. V. Bykova, D. Y. Ermakov, V. V. Kaichev, O. A. Bulavchenko, A. A. Saraev, M. Y. Lebedev and V. A. Yakovlev, Appl Catal B-Environ, 2012, 113, 296-307.
14 B. Q. Xu, J. M. Wei, Y. T. Yu, Y. Li, J. L. Li and Q. M. Zhu, J Phys Chem B, 2003, 107, 5203-5207.
15 C. S. Song, Catalysis Today, 2006, 115, 2-32.
16 P. Q. Liao, W. X. Zhang, J. P. Zhang and X. M. Chen, Nat Commun, 2015, 6, 8697.
17 N. Hosseinpour, A. A. Khodadadi, A. Bahramian and Y. Mortazavi, Langmuir, 2013, 29, 14135-14146.
18 Y. Kazemzadeh, S. E. Eshraghi, K. Kazemi, S. Sourani, M. Mehrabi and Y. Ahmadi, Industrial & Engineering Chemistry Research, 2015, 54, 233-239.
19 J. Liu, P. Chen, L. H. Deng, J. He, L. Y. Wang, L. Rong and J. D. Lei, Scientific Reports, 2015, 5, 15576.
20 C. Franco, E. Patino, P. Benjumea, M. A. Ruiz and F. B. Cortes, Fuel, 2013, 105, 408-414.
21 F. López-Linares, L. Carbognani, M. F. González, C. Sosa-Stull, M. Figueras and P. Pereira-Almao, Energy & fuels, 2006, 20, 2748-2750.
22 N. N. Nassar, A. Hassan and G. Vitale, Applied Catalysis A: General, 2014, 484, 161-171.
23 ChemDraw V14 Structural Drawing Software, in: CambridgeSoft Corporation, a subsidiary of PerkinElmer, Inc, 2014.
24 H. Groenzin and O. C. Mullins, Energy & Fuels, 2000, 14, 677-684.
25 T. W. Mojelsky, T. M. Ignasiak, Z. Frakman, D. D. Mcintyre, E. M. Lown, D. S. Montgomery and O. P. Strausz, Energy & Fuels, 1992, 6, 83-96.
26 A. Devard, R. Pujro, G. de la Puente and U. Sedran, Energy & Fuels, 2012, 26, 5015-5019.
27 JADE V 7.5.1 XRD, Pattern Processing Identification & Quantification, Materials Data Inc. 2005.
28 Ma, D., Investigation into the dielectric behavior of titanium dioxide/polyethylene nanocomposites. Rensselaer Polytechnic Institute: 2003.
29 R. Mueller, H. K. Kammler, K. Wegner and S. E. Pratsinis, Langmuir, 2003, 19, 160-165.
30 A. Hassan, F. Lopez-Linares, N. N. Nassar, L. Carbognani-Arambarri and P. Pereira-Almao, Catalysis Today, 2013, 207, 112-118.
31 P. A. Mulheran, Philos Mag A, 1993, 68, 799-808.
32 M. Yan, S. P. Chen, T. E. Mitchell, D. H. Gay, S. Vyas and R. W. Grimes, Philos Mag A, 1995, 72, 121-138.
33 M. B. Taylor, C. E. Sims, G. D. Barrera, N. L. Allan and W. C. Mackrodt, Physical Review B, 1999, 59, 6742-6751.
34 P. M. Oliver, G. W. Watson and S. C. Parker, Physical review. B, Condensed matter, 1995, 52, 5323-5329.
35 A. Barbier, C. Mocuta, H. Kuhlenbeck, K. F. Peters, B. Richter and G. Renaud, Physical Review Letters, 2000, 84, 2897-2900.
36 A. Wander, I. J. Bush and N. M. Harrison, Physical Review B, 2003, 68, 233405.
37 C. A. J. Fisher, Scripta Materialia, 2004, 50, 1045-1049.
38 J.-E. Jørgensen, L. Mosegaard, L. E. Thomsen, T. R. Jensen and J. C. Hanson, Journal of Solid State Chemistry, 2007, 180, 180-185.
39 BIOVIA Materials Studio Modeling and Simulation Software Version 7.0, Dassault Systemes, San Diego, California, USA, 2014. Home page: http://accelrys.com/products/materials-studio/. 2014.
40 S. Kirkpatrick, C. D. Gelatt, Jr. and M. P. Vecchi, Science, 1983, 220, 671-680.
41 V. Černý, J Optim Theory Appl, 1985, 45, 41-51.
42 L. F. Zhao, L. C. Liu and H. Sun, J Phys Chem C, 2007, 111, 10610-10617.
43 M. J. McQuaid, H. Sun and D. Rigby, J Comput Chem, 2004, 25, 61-71.
44 K. S. W. Sing, D. H. Everett, R. A. W. Haul, L. Moscou, R. A. Pierotti, J. Rouquerol and T. Siemieniewska, in Handbook of Heterogeneous Catalysis, Wiley-VCH Verlag GmbH & Co. KGaA, 2008, DOI: 10.1002/9783527610044.hetcat0065.
45 K. S. W. Sing, Pure and Applied Chemistry, 1982, 54, 2201-2218.

46 V. Biju and M. A. Khadar, Spectrochimica acta. Part A, Molecular and biomolecular spectroscopy, 2003, 59, 121-134.
47 X. Sheng, I. S. U. M. Science and Engineering, Polymer Nanocomposites for High-temperature Composite Repair, Iowa State University, 2008.
48 M. Abboud, M. Turner, E. Duguet and M. Fontanille, Journal of Materials Chemistry, 1997, 7, 1527.
49 I. Langmuir, Journal of the American Chemical Society, 1916, 38, 2221-2295.
50 M. D. Levan and T. Vermeulen, J Phys Chem-Us, 1981, 85, 3247-3250.